Structural Dynamics and Topology of Phospholamban in Oriented Lipid Bilayers Using Multidimensional Solid-State NMR[†]

N. J. Traaseth,[‡] J. J. Buffy,[‡,§] J. Zamoon,[‡,§] and G. Veglia*[,‡,§]

*Department of Chemistry and Department of Biochemistry, Molecular Biology, and Biophysics,
University of Minnesota, Minneapolis, Minnesota 55455*

Received April 19, 2006; Revised Manuscript Received July 15, 2006

ABSTRACT: Phospholamban (PLN), a single-pass membrane protein, regulates heart muscle contraction and relaxation by reversible inhibition of the sarco(endo)plasmic reticulum Ca-ATPase (SERCA). Studies in detergent micelles and oriented lipid bilayers have shown that in its monomeric form PLN adopts a dynamic L shape (bent or T state) that is in conformational equilibrium with a more dynamic R state. In this paper, we use solid-state NMR on both uniformly and selectively labeled PLN to refine our initial studies, describing the topology and dynamics of PLN in oriented lipid bilayers. Two-dimensional PISEMA (polarization inversion spin exchange at the magic angle) experiments carried out in DOPC/DOPE mixed lipid bilayers reveal a tilt angle of the transmembrane domain with respect to the static magnetic field, of $21 \pm 2°$ and, at the same time, map the rotation angle of the transmembrane domain with respect to the bilayer. PISEMA spectra obtained with selectively labeled samples show that the cytoplasmic domain of PLN is helical and makes an angle of $93 \pm 6°$ with respect to the bilayer normal. In addition, using samples tilted by 90°, we find that the transmembrane domain of PLN undergoes fast long-axial rotational diffusion about the bilayer normal with the cytoplasmic domain undergoing this motion and other complex dynamics, scaling the values of chemical shift anisotropy. While this dynamic was anticipated by previous solution NMR relaxation studies in micelles, these measurements in the anisotropic lipid environment reveal new dynamic and conformational features encoded in the free protein that might be crucial for SERCA recognition and subsequent inhibition.

Phospholamban (PLN)[1] is a 52-residue integral membrane protein involved in the uptake of calcium into cardiac sarcoplasmic reticulum (SR). Calcium is pumped into SR vesicles by the sarco(endo)plasmic reticulum calcium ATPase (SERCA), stimulating relaxation of cardiac muscle. PLN inhibits SERCA, by decreasing the calcium affinity for the ATPase and thereby shifting the calcium cooperativity curve. The importance of this protein stems from its pivotal role at the crossroad of two vital physiological pathways: calcium signaling and β-adrenergic stimulation, central mechanisms for the beat-to-beat regulation of heart muscle.

PLN is thought to exist in a dynamic equilibrium between a storage form (pentamer) and an active form (monomer) (*1*, *2*). SERCA has been shown to depolymerize the pentamer, leading to the monomeric form wrapping around SERCA, inhibiting calcium ion translocation (*3*). Calcium flux is restored upon β-adrenergic stimulation leading to PLN phosphorylation at Ser16 and Thr17 by protein kinase A and calmodulin-dependent protein kinase II, respectively (*4*).

The relatively small size and biological importance have made PLN an ideal molecule for understanding membrane protein structure and dynamics. Among the many structural models in the literature, PLN has been proposed to exist as a continuous α-helix (*5*), a transmembrane α-helix with a completely unstructured N-terminus (*6*), and an L-shaped conformation with the cytoplasmic domain interacting with the lipid bilayer (*7*−*9*).

Our effort has focused on the characterization of the monomeric, fully functional AFA-PLN mutant (C36A, C41F, C46A) in both micellar and oriented lipid bilayer systems. All our data consistently point toward the L-shaped arrangement, revealing PLN to be comprised of an amphipathic cytoplasmic helix (domain Ia, residues 1−16), a structured yet flexible loop or hinge region (residues 17−21), and a transmembrane structural domain, which has been further subdivided into two dynamic regions: a more mobile domain Ib (residues 22−30) and a relatively rigid domain II (residues 31−52) (*10*, *11*).

Our dynamic L-shaped model indicates that in the absence of SERCA the cytoplasmic portion of PLN is primarily in contact with the lipid bilayer surface (>90%) but that two

* To whom correspondence should be addressed: Department of Chemistry, University of Minnesota, 139 Smith Hall, 207 Pleasant St. SE, Minneapolis, MN 55455. Phone: (612) 625-0758. Fax: (612) 626-2089. E-mail: veglia@chem.umn.edu.
‡ Department of Chemistry.
§ Department of Biochemistry, Molecular Biology, and Biophysics.
[1] Abbreviations: PLN, phospholamban; PISEMA, polarization inversion spin exchange at the magic angle; SLN, sarcolipin; SERCA, sarco(endo)plasmic reticulum Ca-ATPase.

conformational PLN states (R and T) exist, supported by solution NMR and EPR data (*12, 13*). Additional EPR, fluorescence, CD, and solid-state NMR data recorded in other laboratories (*14, 15*) as well as the amphipathic nature of the cytoplasmic region support these results. Since the surrounding lipids influence the membrane protein function, it is important to determine the overall topology of PLN in order to reveal its interactions with the lipid membrane.

This study not only resolves the inconsistencies in the literature regarding the helicity of the cytoplasmic domain of PLN, showing unambiguous evidence for the presence of a helical conformation, but also elucidates the topology and dynamics in a native lipid bilayer.

MATERIALS AND METHODS

Protein and Sample Preparation. A fully functional monomeric mutant of PLN was used, in which the three transmembrane domain cysteine residues were replaced with alanine, phenylalanine, and alanine (AFA). Selectively labeled ([^{15}N-Ala], [^{15}N-Ile], and [^{15}N-Leu]) and [U-^{15}N]-AFA-PLN were expressed and purified recombinantly as previously described (*16*). PLN (4 mg) was reconstituted in a 10% SDS detergent solution. A 4:1 molar mixture of 1,2-dioleoyl-*sn*-glycero-3-phosphocholine (DOPC) and 1,2-dio-leoyl-*sn*-glycero-3-phosphoethanolamine (DOPE) from Avan-ti Polar Lipids (Alabaster, AL) were dried from chloroform to a thin film, resuspended in water (0.5%, w/v), and sonicated on ice using a micro-tip to form small unilamellar vesicles (SUVs). After sonication, the lipids were centrifuged for 10 min on a benchtop centrifuge at 13K rpm to remove metal and larger vesicles. PLN was added to the lipid mixture followed by one freeze−thaw cycle. The sample was then dialyzed to remove all SDS, concentrated to approximately 2 mL, and deposited onto 40 glass plates (5.7 mm × 12 mm × 0.030 mm; Matsunami, Osaka, Japan). Samples were slowly dried over 2 h at 40 °C, rehydrated for 2 days so that they reached the liquid crystalline phase, and finally sealed in a rectangular glass cell. The final lipid:protein molar ratio for all samples was 200:1.

NMR Spectroscopy. The two-dimensional (2D) polariza-tion inversion spin exchange at the magic angle (PISEMA) was performed (*17,38*) with TPPM decoupling during acquisition (*18*). PISEMA experiments were acquired with 1K scans and 48 t_1 increments for [U-^{15}N]AFA-PLN, 3K scans and 13 increments for [^{15}N-Leu]- and [^{15}N−Ile]AFA-PLN, and 12K scans and eight t_1 increments for [^{15}N-Ala]-AFA-PLN at 4 °C, using a recycling delay of 4 s. All PISEMA data were acquired at a field strength of 14.1 T (^{1}H frequency of 600.1 MHz) equipped with a Bruker DMX spectrometer (National High Magnetic Field Laboratory, Tallahassee, FL). Cross-polarization and SEMA were both performed at 63 kHz using a low-E probe utilizing a doubly tuned, low-inductance resonator built by the RF program at the National High Magnetic Field Laboratory.[2] Data were processed with NMRPipe (*19*) and analyzed using NMR-VIEW (*20*). An exponential window function was applied to the raw data utilizing 50 Hz line broadening along the ^{15}N
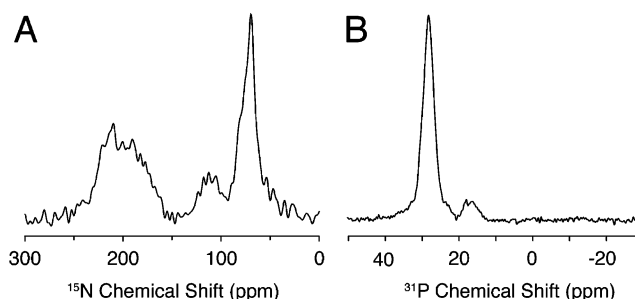
FIGURE 1: (A) One-dimensional ^{15}N spectra of recombinant [U-^{15}N]-AFA-PLN reconstituted into 4:1 DOPC/DOPE lipid bilayers (left). (B) Representative ^{31}P spectra indicating alignment of the bilayer with respect to the static field (right).

chemical shift dimension (t_2). After Fourier transformation and zero-filling, the data consisted of a total matrix size of 2K × 1K points.

Dynamics experiments were performed by acquiring one-dimensional (1D) ^{15}N and PISEMA experiments with the membrane bilayer normal oriented with an angle (α) of 90° with respect to B_0. Experiments with [^{15}N-Leu]AFA-PLN were acquired with 1K scans for 1D experiments and 896 scans and 20 increments for PISEMA. [U-^{15}N]AFA-PLN samples were acquired with 512 scans for the 1D ^{15}N spectrum at $\alpha = 90°$.

RESULTS

Determination of Phospholamban Topology within a Bilayer. Figure 1 shows a 1D ^{15}N spectrum of [U-^{15}N]AFA-PLN and a 1D ^{31}P spectrum of the DOPC/DOPE bilayers, indicating homogeneous alignment of the protein and the lipid bilayers. Within the ^{31}P spectrum, the presence of the peak at 25 ppm indicates that an oriented lipid bilayer has formed, while the presence of a small peak at 17 ppm is likely due to the formation of a DOPE rich domain (*21*). From the 1D ^{15}N experiment, three structural regions within the protein are identified: a transmembrane domain (down-field resonances), a structured yet dynamic loop (isotropic ^{15}N shifts), and a cytoplasmic domain (upfield resonances). Although 1D spectra can be used to interpret topology, a 2D PISEMA spectrum more definitively reveals helical topology within the bilayer (*22*).

In analogy with the assignment strategy by Cross and co-workers (*23*), we have implemented a PISEMA fitting program (*24*), utilizing the tilt (θ) and rotation (ρ) angles of the helix in the bilayer as well as the angle describing the N−H bond vector with respect to the helical axis (δ). These angles along with the periodicity of the helix and residue number are given in a single equation. This approach uses the periodic, wheel-like patterns first identified by Opella and co-workers termed "PISA wheels" (*22*). From these wheels, periodicity, secondary structure, topology, and reso-nance assignments can be assessed simultaneously (*22, 23*).

Figure 2 shows the PISEMA spectrum of [U-^{15}N]AFA-PLN reconstituted in 4:1 DOPC/DOPE bilayers. Our fitting algorithm matches the amplitude of the chemical shift aniso-tropy and dipolar couplings for the PISA wheels correspond-ing to both the cytoplasmic and transmembrane domains, thereby determining the tilt angle with respect to the bilayer normal by minimizing the score function (for details, see ref *24*). This best fit match is shown in Figure 2B
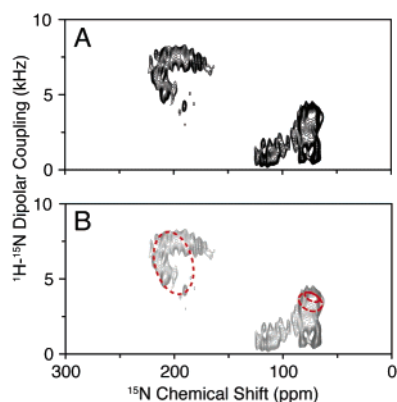
FIGURE 2: (A) PISEMA spectrum of [U-^{15}N]AFA-PLN at a ^{1}H Larmor frequency of 600 MHz. (B) Best fit simulations (dotted, red wheels) to the PISEMA data revealing the helical topology of the transmembrane (21 ± 2°) and cytoplasmic (93 ± 6°) domains with respect to the lipid bilayer normal. The errors of 2° and 6°, respectively, are based on the score function used in the program to match the amplitude of the PISEMA spectrum with that expected for an ideal helix. This error also reflects two additional PISEMA spectra of [U-^{15}N]AFA-PLN.
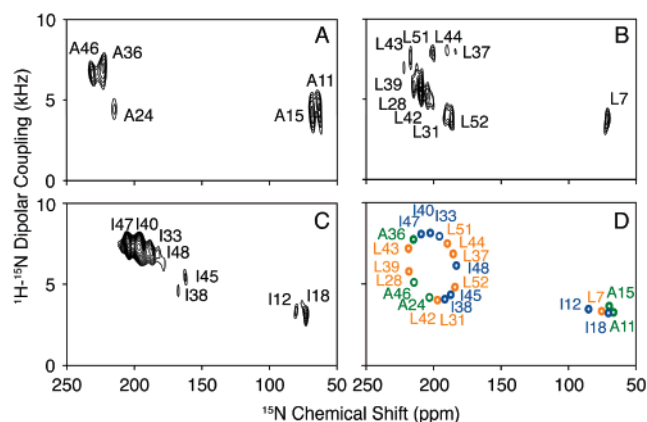

FIGURE 3: PISEMA spectra of [^{15}N-Ala]-, [^{15}N-Leu]-, and [^{15}N-Ile]AFA-PLN (panels A, B, and C, respectively). There are five alanines (two cytoplasmic and three transmembrane domain), eight isoleucines (two cytoplasmic and six transmembrane domain), and 10 leucines (one cytoplasmic and nine transmembrane domain) within AFA-PLN. All spectra were acquired at a ^{1}H Larmor frequency of 600 MHz. (D) Simulated PISEMA spectra shown for selective labels (alanine, isoleucine, and leucine) given the calculated tilt and rotation angle in the bilayer shown in Figure 4.

as indicated by the dotted, red wheels. The helical behavior of residues within the transmembrane domain is apparent by the wheel-like pattern of the spectrum. When all downfield resonances are used as input in the simulation, the best fit to the helical pattern occurs for a transmembrane domain tilt of 21 ± 2° with respect to the bilayer normal.

Deviation from ideal helical structure and protein dynamics can further complicate the assignment of the wheel-like pattern. Therefore, due to the clustering of cytoplasmic domain residues around ∼70 ppm, caused by dynamics and spectral overlap, selectively labeled spectra were required to assign the specific peaks and to identify the helical pattern.

Figure 3 shows PISEMA spectra acquired for [^{15}N-Ala]-, [^{15}N-Leu]-, and [^{15}N-Ile]AFA-PLN samples. AFA-PLN has a total of five alanines: three located in the transmembrane domain and two in the cytoplasmic region. The orientations
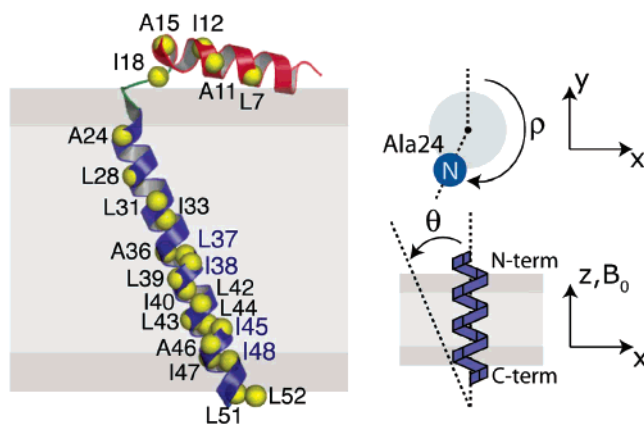

FIGURE 4: Model illustrating the tilt angles of the two domains of PLN (PDB entry 1N7L) (7) determined by PISEMA within the bilayer as well as the rotational angle of the transmembrane domain within the bilayer. In this model, residues Leu31, Ile38, and Ile45 face the lipid membrane. From the definition of the rotation angle within the figure, ρ = 205°.

of Ala11, Ala15, and Ala36 were previously identified by 1D ^{15}N chemical shift spectra using synthetic PLN (10). In the PISEMA spectrum (Figure 3A), all of the resonances are resolved, identifying both chemical shift anisotropy and dipolar couplings for each residue. We repeated the same analysis for both the [^{15}N-Leu]- and [^{15}N-Ile]AFA-PLN samples. Of the 10 leucines present in the PLN primary sequence, nine are located in the transmembrane domain and resonate at low fields, while Leu7 is in the cytoplasmic domain resonating in the upfield portion of the spectrum (Figure 3B). Finally, of the eight isoleucines present in PLN, six are in the transmembrane domain and two in the cytoplasmic domain (Figure 3C). Assignments were made on the basis of matching the best fit of all the experimental selectively labeled resonances to those resonance positions expected for an ideal α-helix. This strategy allows for a unique solution, which has previously been shown to be reliable on the basis that the protein is helical (24).

The assignments of the five residues in the cytoplasmic domain (Leu7, Ala11, Ala15, Ile12, and Ile18) match with the periodicity (i.e., chemical shifts and dipolar couplings) expected for a helix lying on the membrane plane, demonstrating that the cytoplasmic domain is helical in lipid bilayers. The clustering of resonances within the cytoplasmic domain indicates that the tilt angle with respect to the bilayer normal is 93 ± 6°, a result which is in agreement with our predictions using only chemical shift anisotropy data from selective alanine labels (10).

These new solid-state data are highly complementary to the solution studies and help identify the relative orientation and rotation angle of the transmembrane domain of PLN. Figure 4 illustrates the rotation angle (ρ) with respect to the lipid bilayer for the transmembrane domain, showing that residues Leu31, Ile38, and Leu45 face the hydrophobic side of the amphipathic cytoplasmic domain. From the definition of the rotation angle within Figure 4, $\rho \sim 205°$.

While the poor dispersion of cytoplasmic resonances prevented the accurate determination of the rotation angle for the cytoplasmic domain helix, the PISEMA simulations revealed a tilt angle of ∼90° with respect to the bilayer normal. Although additional experimental data are needed
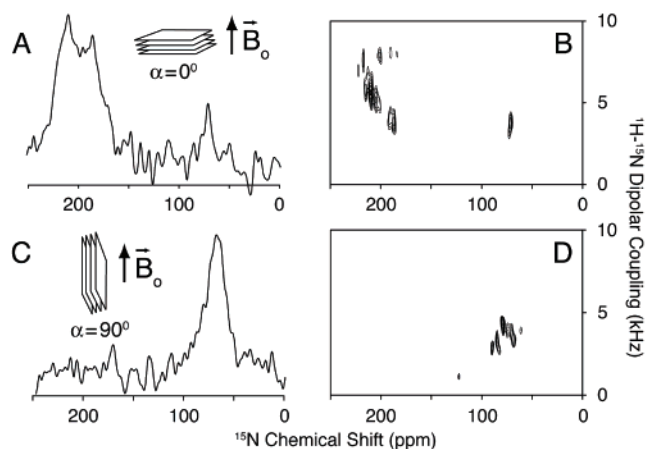
FIGURE 5: (A and C) One-dimensional ¹⁵N spectra and (B and D) PISEMA spectra. (A and B) [¹⁵N-Leu]AFA-PLN with α = 0° and (C and D) α = 90° samples. The presence of discrete resonances in the PISEMA at α = 90° indicates fast motion of the transmembrane domain helix on the NMR time scale.

to accurately determine the rotation angle, the clustering of cytoplasmic domain resonances in the upfield portion of the spectrum strongly supports the conclusion that the cytoplasmic domain is helical and in contact with the surface of the lipid bilayer.

Fast Long-Axial Rotational Dynamics of Monomeric Phospholamban in Oriented Lipid Bilayers. Resonances in PISEMA and 1D ¹⁵N spectra on aligned samples are affected by mosaic spread (nonuniform alignment of the molecule), conformational changes, topological interconversion, and local dynamics (*25*). Although it may be difficult to deconvolute these effects, measuring solid-state spectra with samples oriented at different angles with respect to the direction of the static field (B_o) helps identify rotational dynamics in uniaxially aligned samples (*26−28*).

The canonical orientation used for mechanically aligned samples is with the normal of the bilayer parallel to B_o, which we refer to as α = 0°. When a protein aligned with its helical axis parallel to the membrane bilayer plane at a 0° orientation undergoes long-axial rotation around the bilayer normal, there are no changes to the resonance position. However, when the sample is tilted by 90° (α = 90°), the projection that the N−H bond vectors make with the static field becomes time-dependent with respect to the rotational dynamics, resulting in an effect on line shape and resonance position. If the time scale of the long-axial rotational diffusion is slow, all possible orientations sampled by the rotating molecule will be observed. However, if the rotational diffusion is fast ($<10^{-5}$ s), then both scaling of the chemical shift and dipolar coupling will occur, reducing the powderlike spectrum to a single resonance.

Figure 5 shows 1D ¹⁵N spectra for [¹⁵N-Leu]AFA-PLN at α = 0° and 90°. The [¹⁵N-Leu]AFA-PLN sample was used to identify transmembrane domain residues in the spectrum at α = 90°, since 9 of 10 leucine residues are located within the transmembrane domain. As expected, for α = 90°, leucine residues located in the transmembrane domain shifted to the upfield region of the spectrum. Under these conditions, the transmembrane domain (that has θ = 21° for α = 0°) will assume all possible angles from 69° to 111° with respect to the static magnetic field. If PLN were static, each orien-
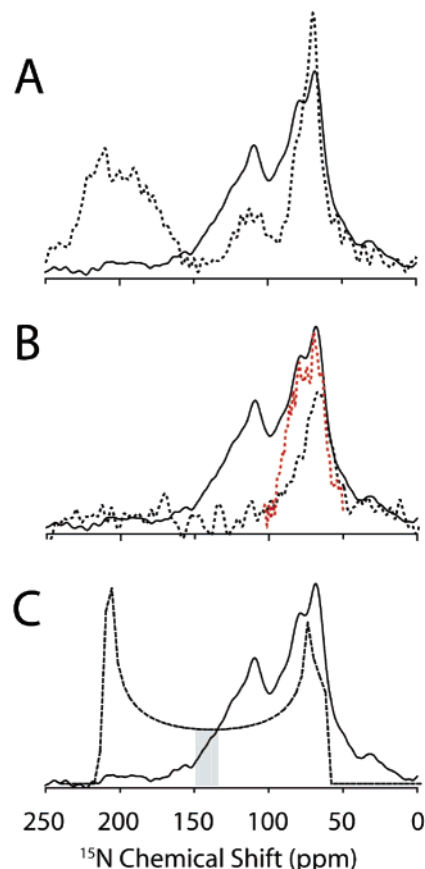

FIGURE 6: (A) One-dimensional ¹⁵N spectra of [U-¹⁵N]AFA-PLN acquired at α = 0° (—) and α = 90° (···). (B) Overlay of the spectrum of [U-¹⁵N]AFA-PLN at α = 90° (—), the spectrum of [¹⁵N-Leu]AFA-PLN at α = 90° (black dotted line), and the mirror image of the downfield resonances of [U-¹⁵N]AFA-PLN at α = 0° (transmembrane domain) scaled by one-half (red dotted line). (C) Overlay of the spectrum of [U-¹⁵N]AFA-PLN at α = 90° (—) and the simulated spectrum of the cytoplasmic domain (···) undergoing slow long-axial rotational diffusion about the membrane normal. The shaded area in panel C indicates the isotropic region of the simulated spectrum for fast long-axial rotational diffusion.

tation would result in a distinct PISEMA pattern, generating a powderlike spectrum. On the contrary, the PISEMA experiment performed with α = 90° shows discrete resonances for the transmembrane domain leucine residues (Figure 5), indicating fast long-axial rotation on the NMR time scale, resulting in spatial averaging (*29, 30*). These results on PLN in lipids are in agreement with Middleton and co-workers (*15*) and EPR results by Thomas and co-workers (*12*). Similar dynamic motion leading to averaged nonaxially symmetric CSA tensors has previously been detected in oriented bilayers and bicelles with ¹⁵N and ¹⁹F nuclei (*27−29, 31*). Furthermore, immobilization of ¹⁹F labels within proteins oriented in lipid bilayers below the main phase temperature (gel phase) has allowed for the measurement of principle tensor components at different tilt geometries of the sample with respect to the static magnetic field (*28*).

While the fast long-axial rotation motion is dominant in the transmembrane domain, the dynamics of the amphipathic, cytoplasmic domain is more complex. Our experiments carried out on AFA-PLN at α = 0° and 90° are summarized in Figure 6. Figure 6A shows 1D ¹⁵N spectra for [U-¹⁵N]-AFA-PLN at α = 0° and 90°. Figure 6B displays the overlay
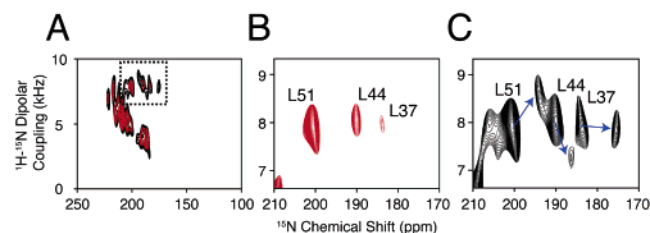
FIGURE 7: (A) Overlay of the PISEMA spectrum for [^{15}N-Leu]-AFA-PLN plotted at two different contour levels. At a higher contour level (red), all of the nine expected leucine resonances are present. At a lower contour level (black), a second set of peaks can be observed. (B and C) Close-up of the rectangle in panel A showing Leu37, Leu44, and Leu51 at higher and lower contour levels, respectively.

of the spectrum of [U-^{15}N]AFA-PLN at $\alpha = 90°$ with both the spectrum of [^{15}N-Leu]AFA-PLN at $\alpha = 90°$ and the mirror image of the transmembrane domain resonances ($\alpha = 0°$) scaled by a factor of one-half. Figure 6C shows the overlay of the spectrum of [U-^{15}N]AFA-PLN at $\alpha = 90°$ with the simulation of slow long-axial rotation diffusion for the cytoplasmic resonances. If the cytoplasmic domain rotated slowly around the membrane normal, a pattern like the simulated spectrum in Figure 6C would be expected. On the other hand, fast rotational motion around the bilayer normal would scale the resonances within the shaded region of Figure 6C. In contrast, the experimental spectrum shown in Figure 6C neither matches the simulated spectrum nor is confined within the shaded region. This indicates that more complex dynamic motions other than fast-axial rotational dynamics exist within the cytoplasmic helix. 1D spectra of [U-^{15}N]AFA-PLN acquired at higher temperatures (unpublished) indicate no further scaling of the line shape at $\alpha = 90°$, meaning that the dynamic motion is at the fast limit on the NMR time scale. From these data, we conclude that PLN motion in oriented lipid bilayers is faster than 10^{-5} s, which is consistent with other spectroscopic measurements (*12, 15, 29*).

Two Topologies of the Transmembrane Domain. In addition to the long-axial rotational diffusion of PLN, PISEMA spectra also map two slightly different topologies within the transmembrane domain. While the presence of conformational dynamics in this domain was anticipated by spin relaxation NMR experiments (*11*), it was not possible to clearly identify this in the isotropically orienting detergent micelles. After a careful analysis of the PISEMA spectra, it is possible to identify two distinct populations of the transmembrane resonances. As an example, the PISEMA spectrum (also reported in Figure 3) of [^{15}N-Leu]AFA-PLN is plotted with a lower threshold (Figure 7A,C). From Figure 7C, it is possible to see a clear doubling of all the resonances. Since this does not depend on the scrambling of the labels during biosynthesis (as assessed by HSQC solution NMR spectra) and it is not attributable to mosaic spread (the resonances would be broadened according to a Gaussian distribution), the peak doubling can be assigned to two topologies of the PLN transmembrane domain. Although these results are preliminary, no change in the tilt angle with respect to the membrane normal for the second population was detected; instead, a small change in the rotational pitch angle (ρ) may describe the second population.

The presence of two different topologies was also observed for PLN transmembrane domains and also reported for sarcolipin (SLN), a highly conserved analogue of PLN that inhibits both SERCA1a and SERCA2a (*24, 39, 40*).

DISCUSSION

The structure of the monomer has been determined in organic solvents, detergent micelles, and lipid bilayers (*6, 7, 9*). Figure 8 summarizes these PLN models in the literature and the expected PISEMA spectra that would arise from these models and topologies.

Although each structure shows PLN's transmembrane domain (residues 22−52) to be helical, each study makes different conclusions regarding the topology and structure for the cytoplasmic domain. Recently, using magic-angle-spinning (MAS) techniques involving through-space and through-bond magnetization transfer techniques, the structure of monomeric PLN was determined in lipid membranes at a lipid:protein molar ratio of 20:1 (*6*). This structure is represented as a model in Figure 8A, with the calculated PISEMA pattern shown in Figure 8F. While the authors concluded that the cytoplasmic domain of PLN is highly dynamic and most likely unstructured, the possibility of a minor population with helical structure was not completely rejected. Although this finding differs from solution NMR and EPR studies in micelles in lipid bilayers, both of which found a major population L-shaped and helical in the cytoplasmic domain (T state) with a minor dynamic population (R state) extended and dynamically disordered (*12, 13*). It is possible that Andronesi et al. with MAS methods probed another minor conformational state of the cytoplasmic domain of PLN. From deconvolution of the EPR signal in lipid bilayers, the percentage of dynamically structured L-shaped PLN was estimated to be 90% (*12*). The existence of a larger population of the T state is most consistent with biological data, indicating both a helical cytoplasmic and transmembrane domain, with the cytoplasmic domain side chain residues involved in phosphorylation (Ser16 and Thr17) facing solvent and the more hydrophobic residues facing the lipid bilayer. The predicted PISEMA data from the L-shaped model shown in Figure 8I best match the experimental PISEMA data (Figure 8J).

Although the lipid environment (charge, curvature, etc.) may play a role in the affinity of the cytoplasmic domain for the bilayer surface and hence its topology, EPR (in DOPC/DOPE lipid vesicles, DPC detergent micelles) (*12, 14*), solution NMR (in DPC detergent micelles) (*7*), and solid-state NMR (in DOPC/DOPE aligned bilayers and DOPC, DOPG, and DMPC vesicles) (*10, 15*) studies conclude that the most preferred topology of PLN is L-shaped with the cytoplasmic domain interacting with the membrane surface.

Interestingly, there are three models for the structure of wild-type PLN (pentameric) where the cytoplasmic domain is helical, but not in contact with the surface of the bilayer (*5, 32*). One model by Smith and co-workers has wild-type PLN modeled as a continuous helix (*5*). A second model by Thomas and co-workers shows PLN to exist in a *pinwheel* assembly where each monomer within the pentamer is L-shaped (*41*). The third and most recent structure by Chou and co-workers (*32*) depicts the pentamer as *bellflower-like*, where the cytoplasmic domain helix of each monomer is
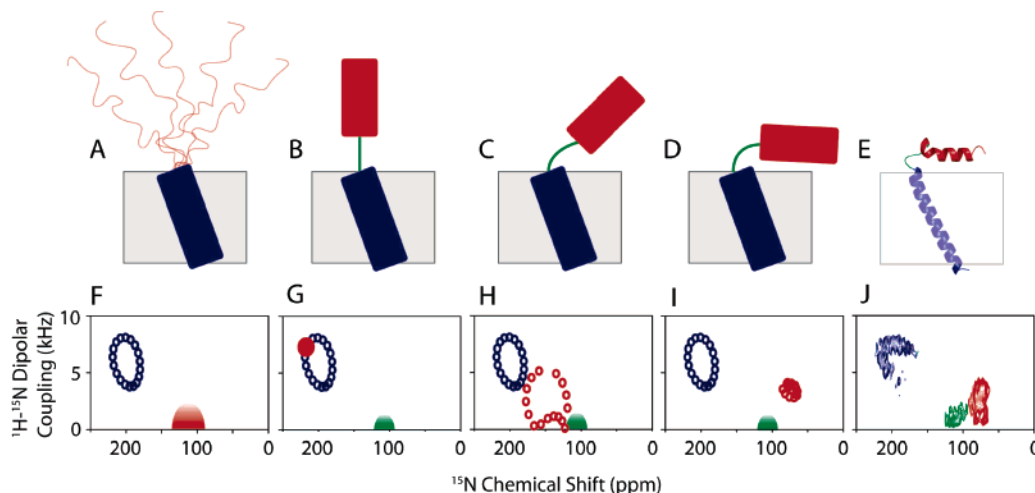
FIGURE 8: Validation of the structural models proposed for PLN in lipid bilayers using PISEMA spectroscopy. The different structural and topological models are shown in panels A−D. The corresponding PISEMA simulations obtained from ideal helices for residues 1−16 and 22−52 are shown in panels F−I. Panel E displays the average minimized structure from the ensemble of conformers reported by our laboratory (PDB entry 1N7L) (7). The colors are coded with the regions of the protein: red for cytoplasmic, blue for transmembrane, and green for loop regions. The half-circular shaded region at ∼117 ppm corresponds to those spectral patterns expected for isotropic motion. The experimental PISEMA spectrum is shown in panel J. The L-shaped structure and topology (panels D and E) and the simulations (panel I) agree best with the experimental PISEMA (panel J).

approximately parallel with the bilayer normal, 90° out of phase from the topology we report for monomeric AFA-PLN. If the cytoplasmic domain of the monomer had an extended structure in agreement with the model proposed for pentameric PLN, one would expect PISEMA spectra corresponding to those simulated in Figure 8G and H, in which the cytoplasmic domain resonances are downfield of the isotropic ^{15}N chemical shift (117 ppm).

This work further supports EPR data in vesicles and solution NMR in detergent micelles showing PLN to primarily exist in a T (or bent) state with the cytoplasmic domain making direct contact with the surface of the bilayer. The angle between the two helical domains of AFA-PLN is ∼66°, with the cytoplasmic domain adopting an angle of 93 ± 6° with respect to the membrane bilayer normal, while the transmembrane domain makes an angle of 21 ± 2° (Figure 4). This topology agrees with our preliminary characterization of PLN based only on chemical shift anisotropy and rigid-body molecular dynamics calculations (10), previous solution NMR studies in organic mixtures (8, 9), and REDOR solid-state NMR experiments reported by Hughes and Middleton (33). In our previous paper, we reported a range of possible solutions for the interhelical angle between 50 and 90° (10). This works stresses the necessity of measuring both chemical shift anisotropy and dipolar couplings for backbone residues in the process of completely determining protein topology.

In addition to the topology, the PISEMA data offer an exquisite view of protein dynamics in oriented lipid bilayers. We have used tilted samples with α = 90° revealing that the cytoplasmic domain of PLN is structured, yet dynamic, undergoing other complex dynamic motion in addition to long-axial rotational diffusion around the membrane normal. The dynamic nature of the cytoplasmic helix was underscored in our micellar studies, where both fast (pico- to nanosecond) and slow (micro- to millisecond) dynamics were detected. In addition to rotational dynamics, our PISEMA spectra also reveal the presence of two populations for the transmembrane

domain, pointing out the importance that solid-state NMR can have in the identification of conformational exchange in an anisotropic environment.

Taken with the sensitivity to point mutation, the dynamics of the transmembrane domain highlights the active role of this region that alone is sufficient for SERCA inhibition. Unlike the transmembrane helix of the diacylglycerol kinase, where every residue can be mutated to both alanine and leucine while maintaining high specific activity, indicating a relatively passive role in the enzyme's structure and function (34), the transmembrane domain of PLN is highly conserved, indicating that both dynamics and structure are needed for proper interaction and inhibition. The presence of two topologies in another protein, SLN (24), a functional homologue to PLN that inhibits both SERCA1a and SERCA2a, underscores the importance of sequence homology for SERCA inhibition.

Solution NMR studies reveal that the transmembrane domains for both PLN and SLN exhibit similar behavior (i.e., unwinding) upon interaction with SERCA (35, 36), which was previously hypothesized by molecular modeling (37). This demonstrates that both sequence and dynamics need to be preserved within PLN and SLN to elicit their similar biological function.

In conclusion, this paper provides a clear picture of the structural dynamics and topology of monomeric PLN in oriented lipid bilayers. Our data show unambiguously that the cytoplasmic domain is helical and lies on the surface of the bilayer, giving monomeric PLN an overall dynamic L-shaped conformation. Moreover, PISEMA spectroscopy shows the presence of two topologies for the transmembrane domain. The dynamics of the cytoplasmic domain and different topologies of the transmembrane domains underscore the importance of a preexisting dynamic equilibrium necessary for the protein's biological function, previously hypothesized on the basis of our NMR studies in an isotropic micellar environment. Solid-state NMR experiments carried out in anisotropic environments reveal new dynamic features

of PLN that will be crucial in understanding the concerted motions and dynamic interplay between SERCA and its inhibitors within native membranes.

ACKNOWLEDGMENT

REFERENCES

1. Arkin, I. T., Adams, P. D., Brunger, A. T., Smith, S. O., and Engelman, D. M. (1997) Structural Perspectives of Phospholamban, a Helical Transmembrane Pentamer, *Annu. Rev. Biophys. Biomol. Struct. 26*, 157−79.

2. Cornea, R. L., Jones, L. R., Autry, J. M., and Thomas, D. D. (1997) Mutation and Phosphorylation Change the Oligomeric Structure of Phospholamban in Lipid Bilayers, *Biochemistry 36*, 2960−7.

3. Kimura, Y., Kurzydlowski, K., Tada, M., and MacLennan, D. H. (1997) Phospholamban Inhibitory Function is Activated by Depolymerization, *J. Biol. Chem. 272*, 15061−4.

4. Simmerman, H. K., Collins, J. H., Theibert, J. L., Wegener, A. D., and Jones, L. R. (1986) Sequence Analysis of Phospholamban. Identification of Phosphorylation Sites and Two Major Structural Domains, *J. Biol. Chem. 261*, 13333−41.

5. Smith, S. O., Kawakami, T., Liu, W., Ziliox, M., and Aimoto, S. (2001) Helical Structure of Phospholamban in Membrane Bilayers, *J. Mol. Biol. 313*, 1139−48.

6. Andronesi, O. C., Becker, S., Seidel, K., Heise, H., Young, H. S., and Baldus, M. (2005) Determination of Membrane Protein Structure and Dynamics by Magic-Angle-Spinning Solid-State NMR Spectroscopy, *J. Am. Chem. Soc. 127*, 12965−74.

7. Zamoon, J., Mascioni, A., Thomas, D. D., and Veglia, G. (2003) NMR Solution Structure and Topological Orientation of Monomeric Phospholamban in Dodecylphosphocholine Micelles, *Biophys. J. 85*, 2589−98.

8. Pollesello, P., Annila, A., and Ovaska, M. (1999) Structure of the 1−36 Amino-Terminal Fragment of Human Phospholamban by Nuclear Magnetic Resonance and Modeling of the Phospholamban Pentamer, *Biophys. J. 76*, 1784−95.

9. Lambeth, S., Schmid, H., Muenchbach, M., Vorherr, T., Krebs, J., Carafoli, E., and Griesinger, C. (2000) NMR Solution Structure of Phospholamban, *Helv. Chim. Acta 83*, 2141−52.

10. Mascioni, A., Karim, C., Zamoon, J., Thomas, D. D., and Veglia, G. (2002) Solid-State NMR and Rigid Body Molecular Dynamics to Determine Domain Orientations of Monomeric Phospholamban, *J. Am. Chem. Soc. 124*, 9392−3.

11. Metcalfe, E. E., Zamoon, J., Thomas, D. D., and Veglia, G. (2004) ^{1}H/^{15}N Heteronuclear NMR Spectroscopy shows Four Dynamic Domains for Phospholamban Reconstituted in Dodecylphosphocholine Micelles, *Biophys. J. 87*, 1−10.

12. Karim, C. B., Kirby, T. L., Zhang, Z., Nesmelov, Y., and Thomas, D. D. (2004) Phospholamban Structural Dynamics in Lipid Bilayers Probed by a Spin Label Rigidly Coupled to the Peptide Backbone, *Proc. Natl. Acad. Sci. U.S.A. 101*, 14437−42.

13. Zamoon, J., Nitu, F., Karim, C., Thomas, D. D., and Veglia, G. (2005) Mapping the Interaction Surface of a Membrane Protein: Unveiling the Conformational Switch of Phospholamban in Calcium Pump Regulation, *Proc. Natl. Acad. Sci. U.S.A. 102*, 4747−52.

14. Karim, C. B., Zhang, Z., and Thomas, D. D. (2006) Phosphorylation-Dependent Conformational Switch in Spin-Labeled Phospholamban Bound to SERCA, *J. Mol. Biol. 358* (4), 1032−40.

15. Clayton, J. C., Hughes, E., and Middleton, D. A. (2005) The Cytoplasmic Domains of Phospholamban and Phospholemman Associate with Phospholipid Membrane Surfaces, *Biochemistry 44*, 17016−26.

16. Buck, B., Zamoon, J., Kirby, T. L., DeSilva, T. M., Karim, C., Thomas, D., and Veglia, G. (2003) Overexpression, Purification, and Characterization of Recombinant Ca-ATPase Regulators for High-Resolution Solution and Solid-State NMR Studies, *Protein Expression Purif. 30*, 253−61.

17. Wu, C. H., Ramamoorthy, A., and Opella, S. J. (1994) High-Resolution Heteronuclear Dipolar Solid-State NMR Spectroscopy, *J. Magn. Reson. 109*, 270−2.

18. Bennett, A. E., Rienstra, C. M., Auger, M., Lakshmi, K. V., and Griffin, R. G. (1995) Heteronuclear Decoupling in Rotating Solids, *J. Chem. Phys. 103*, 6951−8.

19. Delaglio, F., Grzesiek, S., Vuister, G. W., Zhu, G., Pfeifer, J., and Bax, A. (1995) NMRPipe: A Multidimensional Spectral Processing System Based on UNIX Pipes, *J. Biomol. NMR 6*, 277−93.

20. Johnson, B. A., and Blevins, R. A. (1994) A Computer Program for the Visualization and Analysis of NMR Data, *J. Biomol. NMR 4*, 603−14.

21. Henzler Wildman, K. A., Lee, D. K., and Ramamoorthy, A. (2003) Mechanism of Lipid Bilayer Disruption by the Human Antimicrobial Peptide, LL-37, *Biochemistry 42*, 6545−58.

22. Marassi, F. M., and Opella, S. J. (2000) A Solid-State NMR Index of Helical Membrane Protein Structure and Topology, *J. Magn. Reson. 144*, 150−5.

23. Wang, J., Denny, J., Tian, C., Kim, S., Mo, Y., Kovacs, F., Song, Z., Nishimura, K., Gan, Z., Fu, R., Quine, J. R., and Cross, T. A. (2000) Imaging Membrane Protein Helical Wheels, *J. Magn. Reson. 144*, 162−7.

24. Buffy, J. J., Traaseth, N. J., Mascioni, A., Gor'kov, P. L., Chekmenev, E. Y., Brey, W. W., and Veglia, G. (2006) PISEMA Spectra Reveal Topological Interconversion of Sarcolipin in Oriented Lipid Bilayers, *Biochemistry 45* (36), 10939−46.

25. Straus, S. K., Scott, W. R., and Watts, A. (2003) Assessing the Effects of Time and Spatial Averaging in ^{15}N Chemical shift/^{15}N-^{1}H Dipolar Correlation Solid State NMR Experiments, *J. Biomol. NMR 26*, 283−95.

26. Aisenbrey, C., and Bechinger, B. (2004) Investigations of Polypeptide Rotational Diffusion in Aligned Membranes by ^{2}H and ^{15}N Solid-State NMR Spectroscopy, *J. Am. Chem. Soc. 126*, 16676−83.

27. Park, S. H., Mrse, A. A., Nevzorov, A. A., De Angelis, A. A., and Opella, S. J. (2006) Rotational Diffusion of Membrane Proteins in Aligned Phospholipid Bilayers by Solid-State NMR Spectroscopy, *J. Magn. Reson. 178*, 162−5.

28. Grage, S. L., Wang, J., Cross, T. A., and Ulrich, A. S. (2002) Solid-State ^{19}F NMR Analysis of ^{19}F-Labeled Tryptophan in Gramicidin A in Oriented Membranes, *Biophys. J. 83*, 3336−50.

29. Nevzorov, A. A., DeAngelis, A. A., Park, S. H., and Opella, S. J. (2006) NMR Spectroscopy of Biological Solids (Ramamoorthy, A., Ed.) CRC Press: Boca Raton, FL, pp 177−90.

30. De Angelis, A. A., Nevzorov, A. A., Park, S. H., Howell, S. C., Mrse, A. A., and Opella, S. J. (2004) High-Resolution NMR Spectroscopy of Membrane Proteins in Aligned Bicelles, *J. Am. Chem. Soc. 126*, 15340−1.

31. Salgado, J., Grage, S. L., Kondejewski, L. H., Hodges, R. S., McElhaney, R. N., and Ulrich, A. S. (2001) Membrane-Bound Structure and Alignment of the Antimicrobial β-Sheet Peptide Gramicidin S Derived from Angular and Distance Constraints by Solid State ^{19}F NMR, *J. Biomol. NMR 21*, 191−208.

32. Oxenoid, K., and Chou, J. J. (2005) The Structure of Phospholamban Pentamer Reveals a Channel-Like Architecture in Membranes, *Proc. Natl. Acad. Sci. U.S.A. 102*, 10870−5.

33. Hughes, E., and Middleton, D. A. (2003) Solid-State NMR Reveals Structural Changes in Phospholamban Accompanying the Functional Regulation of Ca^{2+}-ATPase, *J. Biol. Chem. 278*, 20835−42.

34. Zhou, Y., Wen, J., and Bowie, J. U. (1997) A Passive Transmembrane Helix, *Nat. Struct. Biol. 4*, 986−90.

35. Traaseth, N. J., Thomas, D. D., and Veglia, G. (2006) Effects of Ser16 Phosphorylation on the Allosteric Transitions of Phospholamban/Ca^{2+}-ATPase Complex, *J. Mol. Biol. 358* (4), 1041−50.

36. Buffy, J. J., Buck-Koehntop, B. A., Porcelli, F., Traaseth, N. J., Thomas, D. D., and Veglia, G. (2006) Defining the Intramembrane Binding Mechanism of Sarcolipin to Calcium ATPase using Solution NMR Spectroscopy, *J. Mol. Biol. 358* (2), 402−9.

37. Toyoshima, C., Asahi, M., Sugita, Y., Khanna, R., Tsuda, T., and MacLennan, D. H. (2003) Modeling of the Inhibitory Interaction of Phospholamban with the Ca^{2+} ATPase, *Proc. Natl. Acad. Sci. U.S.A. 100*, 467−72.

38. Ramamoorthy, A., Wei, Y., and Dong-Kuk, L. (2004) PISEMA Solid-State NMR Spectroscopy, *Annu. Rev. NMR Spectrosc. 52*, 1−52.

39. Hughes, E., Clayton, J. C., and Middleton, D. A. (2005) Probing the Oligomeric State of Phospholamban Variants in Phospholipid Bilayers from Solid-State NMR Measurements of Rotational Diffusion Rates, *Biochemistry 44* (10), 4055−66.

40. Karp, E. S., Tiburu, E. K., Abu-Baker, S., and Lorigan, G. A. (2006) The Structural Properties of the Transmembrane Segment of the Integral Membrane Protein Phospholamban Utilizing (13)C CPMAS, (2)H, and REDOR Solid-State NMR Spectroscopy, *Biochim. Biophys. Acta. 1758* (6), 772−80.

41. Robia, S. L., Flohr, N. C., and Thomas, D. D. (2005) Phospholamban Pentamer Quaternary Conformation Determined by In-Gel Flourescence Anisotropy, *Biochemistry 44* (11), 4302−11.

BI0607610